RSC Advances

ROYAL SOCIETY OF CHEMISTRY

www.rsc.org/advances

RSC Advances

RSCPublishing

ARTICLE

Tunable Field Emission Properties of Well-aligned Silicon Nanowires with Controlled Aspect Ratio and Proximity

Cite this: DOI: 10.1039/x0xx00000x

Received 00th January 2012,
Accepted 00th January 2012

DOI: 10.1039/x0xx00000x

www.rsc.org/

Shasha Lv[a], Zhengcao Li[a*], Shiming Su[a], Linhan Lin[b], Zhengjun Zhang[a], Wei Miao[a]

The size of silicon nanowires (SiNWs) is crucial for their future application in the assembly of field emission (FE) devices. Ag-assisted chemical etching combined with PS sphere as template was employed to prepare size-controllable single crystal SiNWs with uniformity, and the diameter could be further reduced via dry oxidation. The FE properties were found to be strongly influenced by dimensionality and surface geometry structures, and improved progressively with the increase of proximity. The best FE properties was observed in the SiNWs with a tip size of ~ 180 nm (period 1000 nm) and a length of 3.2 μm. It showed a low turn-on field of 1.8 V/μm and a high current density of 0.75 mA/cm^2 at an electric field of 2.5 V/μm. The emission current as a function of time test also demonstrated the good robustness of the SiNWs. The enhanced field emitting efficiency is attributed to the large space between neighboring nanowires, enhanced surface roughness and the sharp tips as hot emission spots.

Introduction

Field emission is one of the most fascinating properties of nanostructured materials, such as silicon nanowires[1-4], carbon nanotubes[5-6], tungsten oxide nanotips[7], SiC needles[8] and ZnO nanowires[9-10]. Due to the complementary metal oxide semiconductor (CMOS) compatibility[11], SiNWs are considered as the potential active electron field emitters and have attracted much attention. Two alternative approaches were utilized to enhance the FE performance of SiNWs - modifying the emitters with surface coating and adjusting dimension of the emitters[12]. Most of the previous efforts have been focused on the heterostructures with various coatings, such as carbon[13-14], graphene[15], ultrananocrystalline (UNCD) diamond film[16], and other metal oxide nanostructures[17]. These procedures used aligned SiNWs templates as high aspect ratio substrates to obtain good electron field emission. However, most of the coatings are not uniformly and densely populated on the SiNWs surface due to the absence of active emission sites. Furthermore, synthesis of these coatings requires sophisticated equipment and complicated processing steps, which limits its application to some extend[16].

It is demonstrated that the geometrical arrangement and dimensional features of SiNWs have a determining influence on the FE properties, and have important consequence for the realization of nanowires field emission devices such as displays[12]. Most of the techniques to prepare SiNWs result in large density and inconformity in distribution[18]. However, FE nanowires device applications require a high degree of precision in position, alignment, and diameters. Thus, how to scale up the synthesis of uniformly aligned and controllable nanowires as field emitters should be further investigated.

In this paper, we discuss a multistep template replication process to fabricate highly periodic and well-aligned silicon nanowires. The diameter could be further controlled via dry oxidation and post chemical treatment[19-20]. To examine the collective size-effects of periodic silicon nanowire (SiNW) arrays, the FE properties related to proximity of as fabricated nanowires were systematically studied. Since this technique combines functionality and economy, it has a high potential to be applied in the field emitters.

Experimental Methods

Nanosphere self-assembly

Figure 1 schematically depicts the procedures used to fabricate the highly ordered and isolated SiNWs. Firstly, the polystyrene monolayer template was prepared on a p-type (100) oriented Si wafer with resistivity below 0.05 Ω cm. The Si pieces were cut and degreased by successive ultrasonic cleaning in acetone, ethanol, and deionized water for 15 min each, and then immersed into boiling Piranha solution (4:1 (*v/v*) H_2SO_4/H_2O_2) for 1 h. The polystyrene (PS) nanospheres solution was diluted with deionized water to the concentration of 0.3 wt % and then mixed with ethanol (1:1 (*v/v*)). The mixture was then

ultrasonicated to ensure the PS spheres well dispersed. The freshly cleaned and superhydrophilic glass slide was mounted in the center of a petri dish, then deionized water was added until the water level was slightly higher than the glass slide's upper surface to make possible the follow-up self-assembly of the PS spheres on the water. Subsequently, the nanaosphere solution was slowly dispersed onto the glass slide. Then several droplets of sodium dodecyl sulfate (SDS) solution (1 wt %) were added to form a compact PS monolayer. Next, pretreated silicon substrates were placed and pushed to the PS sphere side. Finally, after the completion of water evaporation, the monolayer template could be transferred onto the Si substrate upon the completion of water evaporation.

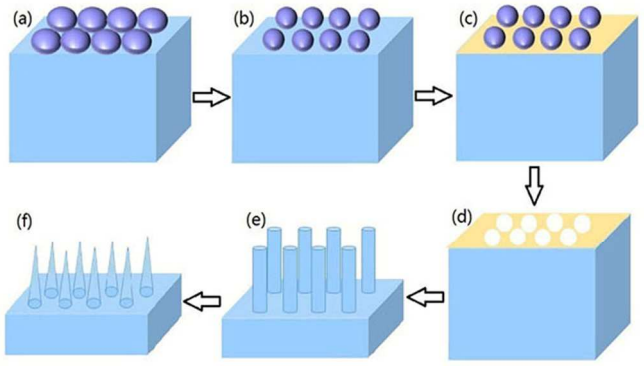

Figure 1. Schematic depiction of the fabrication process. (a) assembly of PS sphere arrays, (b) RIE of the PS spheres, (c) deposition of the Ag film, (d) removal of the PS spheres, (e) metal catalytic etching and removal of the residual silver, (f) dry oxidation and post–chemical treatment

Reactive ion etching (RIE) and Ag deposition

The diameter of the PS sphere was reduced via RIE (Figure 1b), with an O_2 flow rate of 40 sccm, basic pressure of 2 Pa, and applied radio frequency power of 30 W. The etch time was adjusted to control the diameter. After that, Ag was deposited onto the Si substrate by electron-beam evaporation (Figure 1c), forming a porous Ag film as catalyzer. The Ag films used for the chemical etch were deposited at ~ 3 Å s^{-1}. The PS sphere templates were then removed from the substrate by ultrasonication in ethanol or in toluene (Figure 1d).

Metal-catalyzed silicon etch and dry oxidation

The Ag coated Si substrate was etched in a mixture of deionized water, HF, and H_2O_2 at 30 °C for a specified time (5 or 8 min) (Figure 1e). The concentrations of HF and H_2O_2 were 4.8 and 0.3 M, respectively. The retained Ag film was dissolved with nitric acid (1:1 (*v*/*v*) HNO_3/H_2O) for 3 minutes. The diameter of the as-prepared SiNWs was reduced by controlling the dry oxidation time in a tube furnace at 1,050 °C. Finally, the oxide layer was completely removed by post-chemical treatment in the HF solution.

Characterization and Measurement

The morphology and structure of the SiNW arrays were characterized by using the field-emission scanning electron microscope (FE-SEM, JEOL-JSM 7001F, Tokyo, Japan) and transmission electron microscopy (TEM, JEOL-JSM 2011). The field emission properties of SiNWs were measured in a vacuum chamber with base pressures below 2×10^{-5} Pa. The phosphor was deposited on a transparent conductive material (indium-tin-oxide), to serve as the anode electrode in the vacuum system. The distance between the sample and the anode electrode is 200 μm.

Results and Discussion

Figure 2a shows the typical hexagonal close-packed images of PS nanospheres, which have long-range order on the area of several centimeters squared. An oxygen-based RIE was used to reduce the diameter by changing the etching time. The PS spheres with a diameter of 250 nm were reduced to about 170 nm after etching for 75 s, as shown in Figure 2b. Excessive reduction of the sphere size by RIE would prevent the removal of spheres and the chemical etching. After RIE treatment, the spaces between the nanospheres can be utilized for the subsequent Ag film deposition. Figure 2c displays the images of continuous Ag film with a thickness of ~ 35 nm. It should be noted that the thickness of the Ag film must be controlled to ensure both continuity and allow the removal of the PS spheres. After removal of the PS template, the Ag films with regularly distributed hexagonal nanopores of diameters around 173 nm (Figure 2d) were available for chemical etching to obtain the SiNW arrays. It was found that the mean diameter of reactive ion etched spheres, holes on the Ag film and nanowires after metal catalytic etching exhibits an increasing trend during the synthesis process.

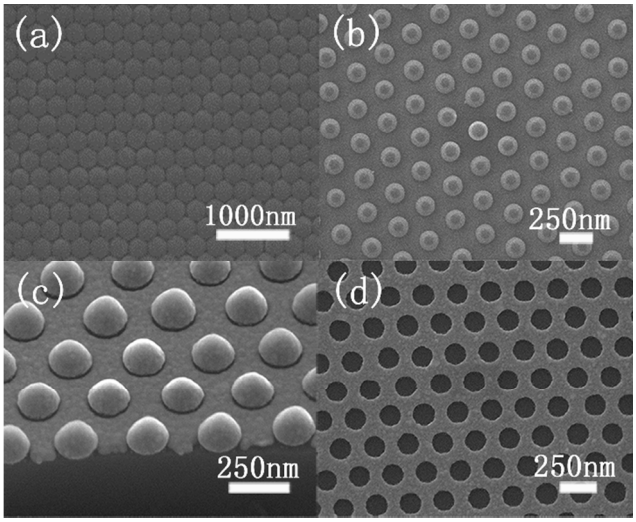

Figure 2. SEM images describing the formation of porous Ag film template. (a) PS spheres with diameter of 250 nm, (b) PS spheres with reduced diameter of 170 nm after RIE treatment for 75 s, (c) Ag film with thickness of 35 nm, (d) Ag hole formed by removal of PS spheres by ultrasonication

Figure 3 shows the cross-sectional SEM images of the well-aligned and uniformly distributed SiNWs resulting from the original PS sphere of 250 nm and their corresponding FE properties. These arrays exhibit good single crystallization,

good alignment and long-range hexagonal periodicity. The mean diameter of the nanowires after Ag-catalyzed chemical etching is 175 nm with a template diameter of 250 nm (Figure 3a). The residual Ag film at the root of the nanowires explicitly confirms the depletion of Ag during the etching process. To reduce the size of SiNWs, dry oxidation and post-chemical etching were carried out. Figure 3b shows that the SiNWs with a diameter of 120 nm were obtained after oxidation of 30 min at 1050 ℃ and post chemical etching of 30 min. A part of these samples was used for the second oxidation for 30 min, and the formed oxide was removed for 30 min. Then, the diameter was further reduced to about 50 nm, as shown in Figure 3c.

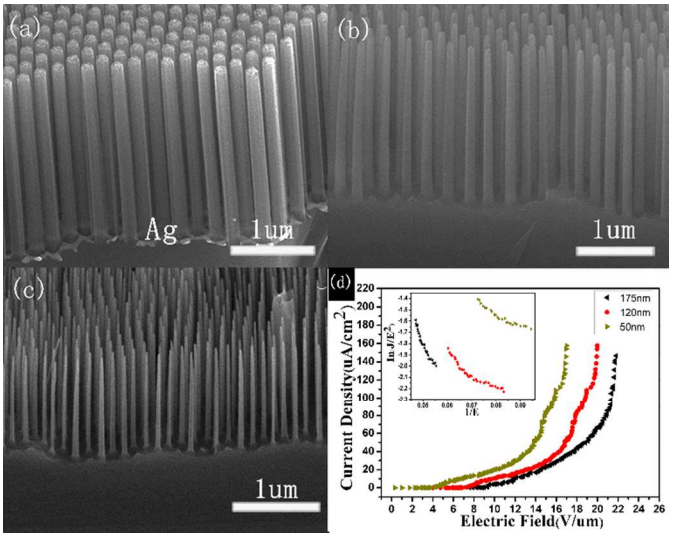

Figure 3. SEM images of SiNW arrays with diameter of (a) 175 nm after 5 min solution etching, (b) 120 nm after 30 min first step oxidation, (c) 50 nm after two-step oxidation for 30+30 min, (d) field emission characteristics of SiNWs resulted from PS spheres of 250 nm.

Figure 3d describes the FE properties of SiNWs correspondent to samples shown in Figures 3a-c. The current density (J) produced by a given electric field (E) is described by the Fowler–Nordheim equation[21]:

$$J = \left(\frac{A\beta^2 E^2}{\Phi}\right)\exp\left(-\frac{B\Phi^{3/2}}{\beta E}\right)$$

Where A and B are constants, Φ is the work function of the emitting materials, β is field enhancement factor. The linear F–N curve plots as In (J/V^2) versus $1/V$, indicating that the field emission is a barrier tunneling quantum mechanical process[22]. Usually, β was calculated from the slope of the F–N plot according to the equation $k = -B\Phi^{1.5}d/\beta$. Here, Φ is 4.64 eV (p-Si (100)), d is the anode–cathode space (200 μm). The SiNWs with diameter of 175 nm exhibit inferior properties. The turn-on field E_0 (electric field required to produce a current density of 10 μA/cm^2) is 11.3 V/μm, and they attain only J＜50 μA/cm^2 at the applied field of 18 V/μm. For SiNWs of 50 nm, the turn-on field and field enhancement factor β value are 7.0 V/μm and 3,119, respectively. It appears that electric field shielding effects from closely packed arrays of nanowires adversely affect their field emission characteristics. Furthermore, the quasi-linear behavior of the inset indicates that the field emission behavior may have a slight deviation from the F-N description, and it could be the influence of the lateral field from other nanowires as well[23].

For further optimization of the FE properties, we need to increase the space between the SiNWs to reduce field shielding effects. The FE performances of SiNWs resulted from 1000 nm PS sphere were studied. Figures 4a, 4b and 4c display the morphology of SiNWs with PS spheres of 1000 nm as template. To improve the aspect ratio, we increased the etching time from 5 min to 8 min, and the corresponding length reaches from 2 μm to approximately 3.2 μm. The mean diameter of SiNWs in Figures 4a and 4b are 590 nm and 480 nm with RIE time of 300 s and 320 s, respectively. To reduce the size of SiNWs, a part of samples shown in Figure 4b was used for dry oxidation for 1 h and post chemical etching for 1 h. The diameters of nanowires increase from 180 nm to 380 nm from top to bottom. The obvious increase from top to bottom result from the uneven etching rate and axially inhomogeneous oxidation rate during the oxidation process.

Figure 4d displays the FE properties of SiNWs with different tip diameters of ~ 590 nm, 480 nm, and 180 nm. The E_0 values with diameters of 480 nm and 590 nm are 5.0 and 3.5 V/μm, respectively. For SiNWs of tip diameters about 180 nm, a high current density of 0.75 mA/cm^2 was obtained at an electric field of 2.5 V/μm with a low turn-on field of 1.8 V/μm. This is superior to the FE properties of other samples. Furthermore, the turn-on field is lower than most SiNWs ever reported[12] and other inorganic semiconductor nanostructures, such as ZnO nanoneedles (2.5 V/μm)[24], ZnS nanobelts (3.47 V/μm)[25], WO_3 nanotips (2.0 V/μm)[26], AlN nanoneedles (2.0 V/μm)[27].

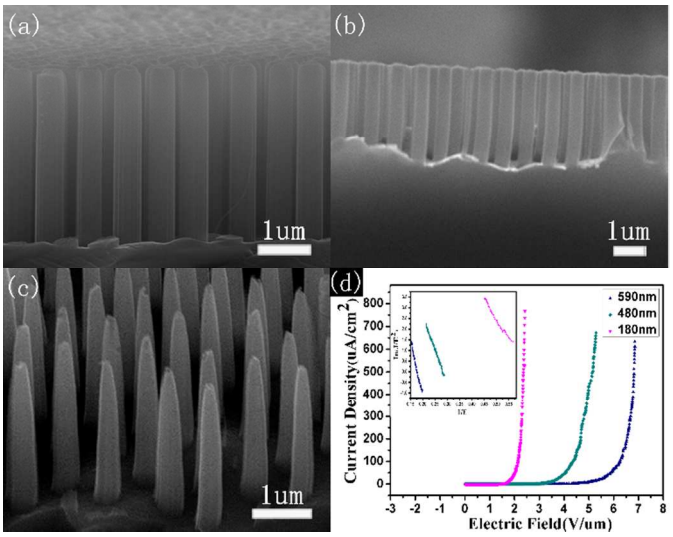

Figure 4. SEM images of SiNW arrays with diameter of (a) 590 nm after 8 min solution etching, (b) 480 nm after 8 min solution etching, (c) tip diameter of 180 nm after 1 h dry oxidation, (d) Field emission characteristics of SiNWs resulted from PS spheres of 1000 nm.

The detailed nanostructures of SiNWs in Figure 4d were further characterized by TEM. Figure 5a shows the nanowire with

diameter ranging from ~180 nm at the tip to ~300 nm at the middle to ~380 nm at the bottom. Figure 5b shows that SiNWs have single-crystalline core shelled with a thin layer of amorphous SiO_2 (~10 nm). Si is susceptible to form native oxide even at ambient conditions. However, the thin SiO_2 shell may contribute the enhanced property due to the small electron affinity[28-29]. Figure 5c shows the enlarged tip region of rough surface and sharp corners, revealing the existing emission sites - hot spots. The roughness of the SiNWs increases emission sites and enhances FE properties[1, 15, 30].

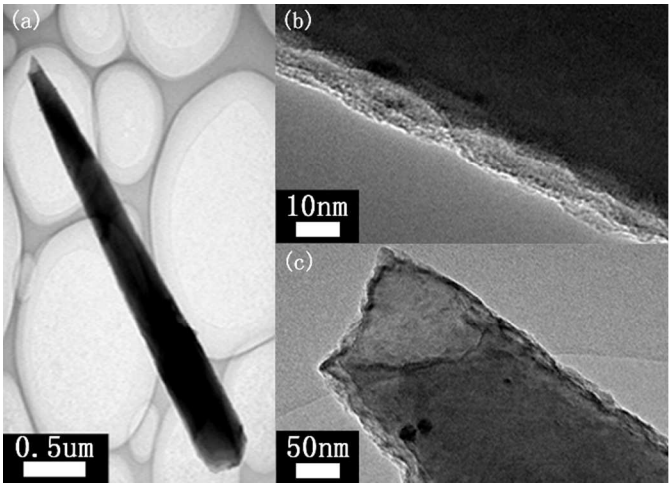

Figure 5. TEM images of SiNWs with the tip size of ~180 nm and the length of 3.2 μm (a) under a low magnification. Typical corresponding images of (b) side region and (c) tip region.

Although quite a few studies on the field emission from SiNWs have been published, only a few of those compare SiNWs of different morphologies. The samples here offer a chance to assess the role of overall geometry of the emitters. The parameters and FE properties of the SiNWs are summarized in Table 1. Because the local electric field at the emission site that governs the emission, we take the tip diameter of 180 nm as their diameter to discuss FE properties of SiNWs. Figure 6 summaries the relationship between FE performances and the proximity of SiNWs. When the space between the SiNWs increases, the turn-on field obviously decreases from 11.3 to 1.8 V/μm. Furthermore, the SiNWs resulted from PS sphere of 1000 nm have lower turn-on field and higher β values than that resulted from PS sphere of 250 nm, suggesting that increases of the distance will effectively reduce the electrostatic shielding among the emitters. Nilsson L *et al.*[31] reported that the nanowires should be separated twice their height in order to reduce field shielding effects thoroughly. Meanwhile, the large space makes the surface density and emission spots decrease. Thus, there is an optimum distance for a maximal emitted current density that amounts to 1-2 times the nanowire distances. However, it is difficult to meet the requirements by usual experiment methods except for the lithography process.

The field enhancement factor β is determined by the geometrical shape and surroundings of the emitters. Although the unit area have more SiNWs with period of 250 nm than that with period of 1000 nm, and the aspect ratio of SiNWs with diameter of 50 nm is larger than other samples, electrostatic shielding among the emitters weakens the field amplification effect to make β reduced. Furthermore, β values reported here are much larger than the ratio between height and radius of curvature of an emitter. This is due to the increment of surface roughness[32-33] and the abundance of emission spots from emitters. Thus, materials with elongated geometry, sharp tips and rough surface can greatly increase the enhancement factor.

Table 1. Key Parameters of SiNWs Field Emitters in This Work

average diameter (nm)	average spacing (nm)	length (μm)	turn-on field (V/μm)	β
50	200	2	7.0	3119
120	130	2	9.9	2010
175	75	2	11.3	1300
180	820	3.2	1.8	5785
480	520	3.2	3.5	4741
590	410	3.2	5.0	3700

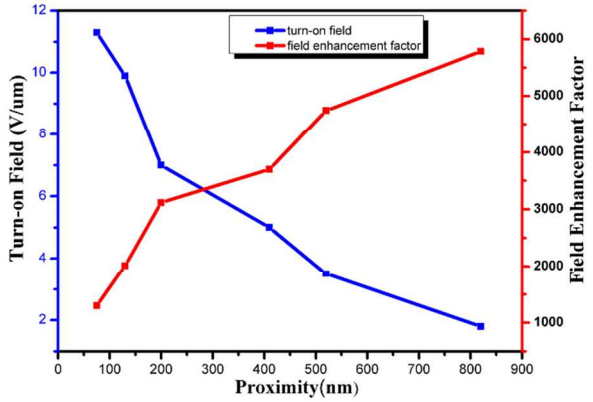

Figure 6. Relationship of turn-on field and field enhancement factor β with proximity.

Finally, to check the robustness of the present SiNWs, the field emission stability of SiNWs with the tip diameter of 180 nm was recorded at a fixed electric field of 2.3 V/μm for 6 h (Figure 7). It shows an average emission current density of 300 uA/cm^2, and the variation of the current density is estimated to be 10.4 %, without showing sign of degradation over the 6 h period. No changes in the morphology after 6 h of continuous emission are observed in the SEM. The stable FE performance discovered in this work is related to uniformity of aligned silicon nanowires, which guarantees a uniform field distribution across the arrays. The emission are explainable that most of

them have a sufficient β factor for an adequate emission. What's more, Field emission is a highly selective process and is extremely sensitive to small variations in the dimensions, and surroundings of the emitters[34]. Thus the morphology of individual SiNWs is indeed of crucial importance for the FE properties.

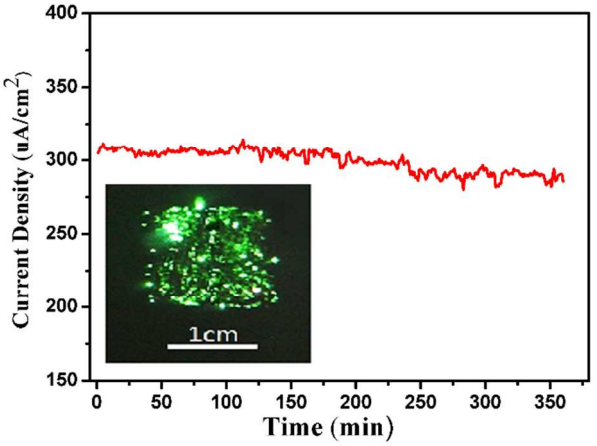

Figure 7. FE stability of SiNWs with the tip diameter of 180 nm, emission current as a function of time, at an applied field of 2.3 V/μm.

Conclusions

We successfully fabricated the high-quality single-crystal SiNWs with excellent conformality and reliability. In order to control the diameter, length and density of SiNWs, template-assisted chemical etching combined with dry oxidation was successfully utilized. The FE properties of SiNWs were systematically studied by using two different polystyrene (PS) spheres template with the original diameters of 250 nm and 1000 nm. A remarkable improvement of turn-on field from 11.3 to 1.8 V/μm was observed with the average tip space increasing from 80 to 820 nm. The field enhancement factor improves progressively, up to 5785. The SiNWs with a tip diameter of 180 nm and height of 3.2 μm showed the lowest emission fields and exhibited favorable FE stability, that is, the emission current fluctuation ~ 10.4 % was observed at a fixed electric field of 2.3 V/μm for 6 h. These results outperform most of other studies on SiNWs at technologically useful current densities. The excellent FE properties are closely related to the uniformly distributed nanowires with large proximity, favorable morphological features and the sharp tips as hot emission spots. It is expected that these SiNWs will become available as CMOS-compatible, effective and low cost field emitters.

Acknowledgments

The authors wish to thank Doctor. Peng Liu from Tsinghua-Foxconn Nanotechnology Research Center for his kind advices and measurements to this work. The central laboratory of Institute of Materials Science and Engineering, Tsinghua University and the National Center for Electron Microscopy (Beijing) are also gratefully acknowledged for supporting the analysis and characterizing of the silicon nanowires in this work. The authors are grateful to the financial support by the Natural Science Foundation of China (61176003 and 61076003).

Notes and references

[a] School of Materials Science and Engineering, Key Laboratory of Advanced Materials, Tsinghua University, Beijing 100084, People's Republic of China
[b] Department of Electrical and Computer Engineering, University of Michigan, Dearborn 47001, Michigan, United States

1. R. R. Devarapalli, R. V. Kashid, A. B. Deshmukh, P. Sharma, M. R. Das, M. A. More and M. V. Shelke, J. Mater. Chem. C, 2013, **1**, 5040-5046.
2. B. Zeng, G. Xiong, S. Chen, S. H. Jo, W. Z. Wang, D. Z. Wang and Z. F. Ren, Appl. Phys. Lett., 2006, **88**, 213108.
3. J. C. She, S. Z. Deng, N. S. Xu and R. H. Yao, J. Chen, Appl. Phys. Lett., 2006, **88**, 013112.
4. B. Zeng, G. Xiong, S. Chen, W. Wang, D. Z. Wang and Z. F. Ren, Appl. Phys. Lett., 2007, **90**, 033112.
5. S. Fan, M. G. Chapline, N. R. Franklin, T. W. Tombler, A. M. Cassell and H. Dai, Science, 1999, **283**, 512-514.
6. N. Shimoi, A. L. Estrada, Y. Tanaka, K. Tohji, Carbon 2013, **65**, 228-235.
7. B. R. Huang, T. C. Lin, K. T. Chu, Y. K. Yang, J. C. Lin, Surf. Coat. Tech., 2013, **231**, 289-292.
8. R. Wu, K. Zhou, X. Qian, J. Wei, Y. Tao, C. H. Sow, L. Wang and Y. Huang, Mater. Lett., 2013, **91**, 220-223.
9. R. R. Devarapalli, D. R. Shinde, F. B. Bouaifel, S. G. Yenchalwar, R. Boukherroub, M. A. More and M. V. Shelke, J. Mater. Chem., 2012, **22**, 22922-22928.
10. C. X. Zhao, K. Huang, S. Z. Deng, N. S. Xu, J. Chen, Appl. Surf. Sci., 2013, **270**, 82-89.
11. V. Schmidt, J. V. Wittemann, S. Senz, U. Gösele, Adv. Mater., 2009, **21**, 2681-2702.
12. X. Fang, Y. Bando, U. K. Gautam, C. Ye and D. Golberg, J. Mater. Chem., 2008, **18**, 509-522.
13. D. Banerjee, N. S. Das and K. K. Chattopadhyay, Appl. Surf. Sci., 2012, **261**, 223-230.
14. N. S. Das, D. Banerjee and K. K. Chattopadhyay, Appl. Surf. Sci. 2011, **257**, 9649-9653.
15. J. H. Deng, B.Yu, G. Z. Li, X. G. Hou, M. L. Zhao, D. J. Li, R. T. Zheng and G. A. Cheng, Nanoscale 2013, **5**, 12388-12393.
16. T. H. Chang, K. Panda, B. K. Panigrahi, S. C. Lou, C. Chen, H. C. Chan, I. N. Lin and N. H. Tai, J. Phys. Chem. C, 2012, **116** (37), 19867-19876.
17. F. Zhao, G. A. Cheng, R. T. Zheng, D. D. Zhao, S. L. Wu, J. H. Deng, Nanoscale Res Lett, 2011, **6**, 176.
18. Y. J. Yang, G. M., X. Y. Liu, L. Zhang, Z. Hu, C. Y. He, and Y. M. Hu. J. Phys. Chem. C 2008, **112**, 20126.
19. Z. Huang, H. Fang and J. Zhu, Adv. Mater. 2007, 19, 744-748.
20. S. M. Su, L. H. Lin, Z. C. Li, J. Y. Feng and Z. J. Zhang. Nanoscale Res Lett, 2013, **8**, 405.
21. T. E. Stern, B. S. Gossling and R. H. Fowler, Proc. R. Soc., 1929, **124** (795), 699-723.

22. R. H. Fowler and L. Nordheim, Proc. R. Soc. 1928, **119**, 173-181.
23. G. Fursey, Appl. Surf. Sci. 1995, **94**, 44-59.
24. Y. B. Li, Y. Bando and D. Golberg, Appl. Phys. Lett., 2004, **84**, 3603.
25. X. S. Fang, Y. Bando, G. Z. Shen, C. H. Ye, U. K. Gautam, P. M. F. J. Costa, C. Y. Zhi, C. C. Tang and D. Golberg,. Adv. Mater., 2007, **19** (18), 2593-2596.
26. J. Zhou, L.Gong, S. Z. Deng, J. Chen, J. C. She, N. S. Xu, R. Yang and Z. L. Wang, Appl. Phys. Lett., 2005, **87**, 223108.
27. Q. Zhao, J. Xu, X. Y. Xu, Z. Wang and D. P. Yu, Appl. Phys. Lett., 2004, **85**, 5331.
28. H. Wang, W. Jiang, L. Kang and Z. Li, J. Alloy. Compd. 2013, **553**, 125-128.
29. Z. J. Qian, X. Y. Liu, Y. Yang and Q. X. Yin, J. Nanosci. Nanotechnol., 2014, **14**, 6209-6212.
30. T. Sugino, T. Hori, C. Kimura and T. Yamamoto, Appl. Phys. Lett., 2001, **78**, 3229.
31. L. Nilsson, O. Groening, C. Emmenegger, O. Kuettel, E. Schaller, L. Schlapbach, H. Kind, J. M. Bonard and K. Kern, Appl. Phys. Lett., 2000, **76**, 2071.
32. N. Koenigsfeld, R. Kalish, A. Cimmino, D. Hoxley, S. Prawer and I. Yamada, Appl. Phys. Lett., 2001, **79**, 1288.
33. T. Sugino, C. Kimura and H. Aoki, Diamond and Related Materials, 2008, **17**, 1764–1769.
34. J. M. Bonard, N. Weiss, H. Kind, T. Stöckli, L. Forró, K. Kern, and A. Châtelain Adv. Mater., 2001, **13** (3), 184-188.

